



A system for identifying an anti-counterfeiting pattern based on the statistical difference in key image regions

Zhaohui Zheng^{a,b}, Hong Zheng^{c,*}, Jianping Ju^d, Deng Chen^e, Xi Li^f, Zhongyuan Guo^c, Changhui You^c, Mingyu Lin^d

^a School of Mathematics and Physics, Wuhan Institute of Technology, Wuhan 430079, China

^b Wuhan Railway Vocational College of Technology, Wuhan 430200, China

^c School of Electronic Information, Wuhan University, Wuhan 430000, China

^d School of Artificial Intelligence, Hubei Business College, Wuhan 430070, China

^e School of Computer Science and Engineering, Wuhan Institute of Technology, Wuhan 430000, China

^f School of Electrical and Information Engineering, Wuhan Institute of Technology, Wuhan 430000, China



ARTICLE INFO

Keywords:

Anti-counterfeiting pattern
Supervised and guided segmentation
Bone width transformation
Key regions

ABSTRACT

An important aspect of identifying whether items are likely to be forged or infringe upon a copyright is the use of an anti-counterfeiting pattern because it can help in determining and detecting forged anti-counterfeiting labels and patterns. At present, most anti-counterfeiting systems require special materials or large samples of images for training. Once they are geometrically attacked or forged by printing and scanning, they will be completely invalid. Therefore, this paper proposes an anti-counterfeiting system that uses a single corresponding feature difference sequence of the key regions for statistical analysis. The aim of our technology is to use the inks to generate random subtle texture patterns, and construct a supervised and guided segmentation algorithm and bone width transformation algorithm to locate the key regions of the sample images, which is used to identify the authenticity of the inspected product. The experiment shows that the system not only has high anti-counterfeiting performance and good robustness but also provides a convenient and practical idea for anti-counterfeiting technology.

1. Introduction

For several years, fake and inferior products have caused serious harm to the world economy and consumers. With the advent of low-cost scanning equipment, high-quality printers and better color copiers, it has become easier to forge anti-counterfeiting patterns. Therefore, the authenticity verification of an anti-counterfeiting pattern is an increasingly important task. To incorporate additional security features, an anti-counterfeiting method often adopted in practice is to add special materials to synthesize anti-counterfeiting patterns (Liu & Xu, 2013). While such methods have good anti-counterfeiting properties, they are costly and interact poorly, and consumers need to learn how to verify and differentiate them. Therefore, a significant research direction is to use the printing characteristics of anti-counterfeiting patterns without adding additional materials with security characteristics (Navarro et al., 2018). The printing effect will differ if a forged anti-counterfeiting

pattern can be printed with different printers, especially at the edge of the geometric pattern. Even using the same printer twice can yield different results, similar to the idea that “there are no two identical leaves in the world”. The inherent differences in these random results do not require any additional means, especially for a single (one to one) corresponding verification, which is very useful.

However, robust extraction by shape features and texture features for verification is a popular topic and difficult problem in the current research. Furthermore, to ensure high accuracy, most professional acquisition equipment can be used for authenticity detection, which cannot meet the public's need for convenient anti-counterfeiting identification. To extract the useful features, remove considerable redundant information from an image, focus on the geometric feature information of the important key regions of an anti-counterfeiting pattern, and solve the need for authenticity recognition of single sample images in practical applications, this paper proposes an authenticity identification system of

* Corresponding author.

E-mail addresses: zhengzhaohui@whu.edu.cn (Z. Zheng), zh@whu.edu.cn (H. Zheng), gjdxjjp@whu.edu.cn (J. Ju), dchen@wit.edu.cn (D. Chen), lixi@wit.edu.cn (X. Li), Guozhongyuan1993@outlook.com (Z. Guo), youchanghui@whu.edu.cn (C. You), limmingyu@hb.edu.cn (M. Lin).

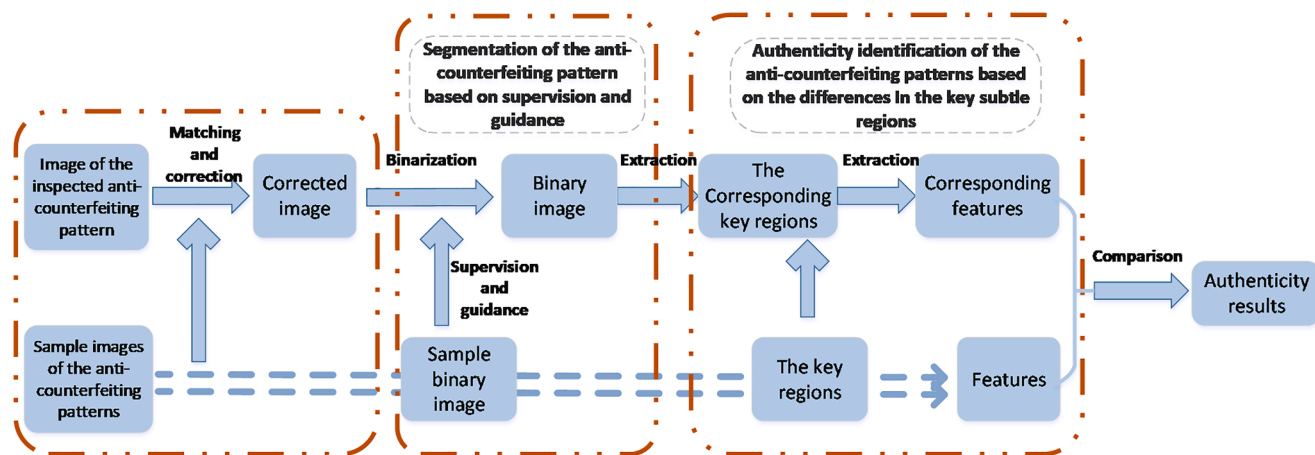


Fig. 1. Flow chart of the anti-counterfeiting algorithm.

anti-counterfeiting patterns, which uses the anti-counterfeit sample patterns and the significant differences between the key regions of the images to identify the authenticity of the inspected anti-counterfeiting pattern. In the anti-counterfeiting pattern printing process, the system abandons the plate-making printing of traditional commodity packaging and adopts a random generation mode so that each product packaging has a unique and noncopyable structural anti-counterfeiting feature. Then, the corresponding anti-counterfeiting labeled digital images are collected as the samples and the information is stored in the query center database so that the authenticity can be identified at any time with smartphones and computers in the Internet environment. In the anti-counterfeiting pattern identification process, to find the best key regions in the anti-counterfeiting pattern, first, binarization processing is carried out on the sample images of the anti-counterfeiting pattern and the image of the inspected anti-counterfeiting pattern after image registration. Bone width transformation is used to extract the subtle region as the key region, and then, the authenticity of the inspected anti-counterfeiting pattern is identified by comparing the differences in key regions; see Fig. 1.

The main highlights of the system proposed in this paper are as follows:

- We adopt a random subtle texture pattern that is generated automatically, with one object per code, which is difficult to forge and has a high cost.
- We propose a threshold segmentation (guide-binary) method for anti-counterfeiting patterns based on supervised guidance, which makes it easier to approach the real segmentation effect than to use the traditional threshold segmentation, thereby ensuring the invariance of subtle regions.
- We propose the bone width transformation (BWT) algorithm, which improves the calculation speed of the texture width, and is beneficial to quickly extract key and subtle regional differences to verify the authenticity of anti-counterfeiting patterns.

2. Review of existing methods

With the popularity of smartphones, the acquisition of high-quality images has become an increasingly easier task and provides the necessary conditions for the rapid development and application of image-based anti-counterfeiting technology. However, there are few public studies directly on automatic identification technology for anti-counterfeiting images, although the research on relevant data models (Alizadeh, Allen, & Mistree, 2020; Soltanisehat, Alizadeh, & Hao, 2020) and images (such as document images, banknote images and seal images) is abundant. Generally, there are two kinds of methods: shape-

based and texture-based authenticity identification.

- Shape-based pattern authenticity identification. Due to the slight geometric distortion of an anti-counterfeiting pattern or a character during printing, the difference in the linear geometric distortion between a true anti-counterfeiting pattern and forged anti-counterfeiting patterns can be measured and correlated by extracting and analyzing the shape region of the anti-counterfeiting pattern with the shape features.

In the authenticity identification of document images, Lampert, Mei, and Breuel (2006) proposed a system that used local features (such as line edge roughness, region difference and correlation coefficient) and focused on a single character image to identify the document images. However, the system can obtain good results by scanning images at a very high resolution (3200 dpi). Gebhardt, Goldstein, and Shafait (2013) proposed an attribution printing system that uses the edge roughness difference to differentiate between document images that ultimately distinguishes between laser printing and inkjet printing. This method uses the standard deviation of the pixel gray value along the vertical edge of the image to calculate the roughness of the edge. Rough edges with large gray variation along the vertical edge will lead to higher standard deviations. Therefore, the standard deviations of all connected regions with the shortest vertical edge are calculated, but it's easily affected by imaging equipment and environmental light, and it needs training data. Umadevi, Agarwal, and Rao (2011) proposed using the expected maximization (EM) algorithm to distinguish the printer types of documents, which were divided based on the character region, background region and noise region through character segmentation; then, the document printers were classified by iterative calculation, but this method can only be used for basic print type recognition. Elkasrawi and Shafait (2014) proposed a method to obtain statistical features from the noise residuals of each character using the unique noise generated by the printer. However, this method is easily affected by the binarization effect when extracting noise. In the authenticity identification of a seal image, Wu, Kong, and Shang (2015) proposed a printer model composed of the distance and angle of halftone points and used the Euclidean distance and k-means to identify printer attributes. However, this method is easily affected by illumination when extracting halftone points, so it is necessary to use a scanner to collect images for recognition. He (2010) proposed a method that uses the difference between the edges to identify authentic and fake seals. In view of the slight difference between authentic and fake seals, the edge geometric difference of the seals was further analyzed, and the

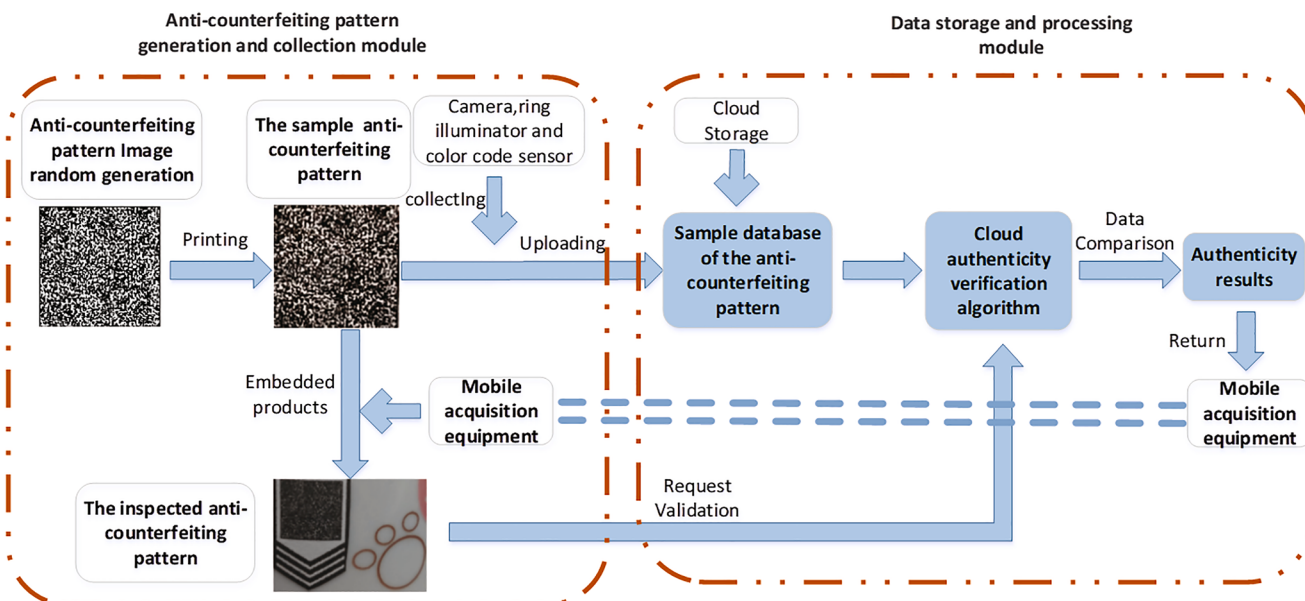


Fig. 2. General framework of the system.

difference value was quantified to form the difference histogram as the feature vector, where the difference was determined by the corresponding edge distance and length between the seals. Finally, a support vector machine (SVM) was used to train and classify the feature vectors. Nevertheless, these methods are easily affected by the effect of edge extraction.

- (2) Texture-based pattern authenticity identification. Because textures can represent the internal details of printed anti-counterfeiting patterns, the research and development of anti-counterfeiting technology based on texture has become an important research field in recent years. The texturing approach relies on pattern flaws between adjacent pixels. These pattern defects are caused by the melting and solidification of toner ink, which is scattered over letters and uneven outlines.

In the authenticity identification of document images, Mikkilineni et al. (2005) used the gray-level concurrence matrix (GLCM) as the feature descriptor of all letters “e”. For each letter “e”, the GLCM estimates 22 statistical features, combined with a simple nearest neighbor classifier (KNN) to make predictions, and then conducts a majority vote to determine the attributive classification of the printed documents. Ferreira, Navarro, Pinheiro, dos Santos, and Rocha (2015) used multidirectional and multi-scale co-occurring texture patterns and a convolutional texture gradient filter (CTGF) as feature descriptors. Navarro et al. (2018) extend upon the CTGF algorithm to analyze, isolate and produce visible and interpretable features, giving rise to the CTGF-Map algorithm. These methods not only needs the same scanning equipment to obtain the document image but can also only process the trained characters. Schreyer, Schulze, Stahl, and Effelsberg (2009) evaluated the authenticity identification of discrete cosine transform (DCT) features for printed documents scanned at low and high resolutions, but the evaluation was not comprehensive, and only one original document was used for testing. Sharad and Khanna (2018) used local texture pattern (LTrP) based features and a single classifier to classify all printed letters. Then, Sharad and Khanna (2019) introduced a new printer-specific local texture descriptor (PSLTD) to capture textures on the scanned image of a printed document. Compared with local binary patterns (LBP), the dimension of Sharad's texture features is greatly increased, which is convenient for subsequent training processing, but it is not suitable for small

sample authenticity identification. Tsai, Yin, Yuadi, and Liu (2014) combined the discrete wavelet transform (DWT) and GLCM, calculated 12 DWT features and 22 GLCM features from each corresponding character, and used an SVM to train and classify the features. Subsequently, in Tsai, Hsu, Yin, and Yuadi (2015), they also used spatial filters, Gabor filters and Wiener filters to calculate more features for classification, but Tsai's method only analyzed the scanned images obtained from the laser printer source. For the authenticity identification of patterns, Cheng (2015) proposed a method that computes the image texture by a DCT. Combined with digital anti-counterfeiting technology, the calculated DCT feature vector is used for texture anti-counterfeiting labels. Finally, the method identifies the image authenticity by calculating the distances between the texture anti-counterfeiting labels. Zhang (2017) evaluated the methods for calculating the image texture features among the DFT, DCT and DFT-DCT and verified the reliability and feasibility of the three methods in the automatic identification of genuine anti-counterfeiting labels. Although noise, zoom and rotation are considered in the experiments, whether the main factors, such as brightness and contrast difference, affect the identification effect has not been analyzed. Researchers use special materials for anti-counterfeiting. For example, Zhong, Li, and Liu (2018) imprinted robust invisible patterns in colloidal crystals of hollow silica spheres. The color of the patterned regions is further independently tuned by vapors with different refractive indices. Wu, Liu, and Su (2017) printed patterns and the background with inks containing uniform CdS spheres with different diameters but similar intrinsic colors, so that the invisible patterns can be observed clearly by simply changing the viewing angle. Hou, Zhang, and Su (2016) presented an anti-counterfeiting strategy. By controlling the rheology of poly(dimethylsiloxane) (PDMS), three kinds of PC dots could be sequentially integrated into one pattern using the layer-by-layer printing strategy. Bae, Bae, and Park (2015) used randomly generated silica film wrinkles to encrypt polymer particles. The generated wrinkle codes are as highly unique as human fingerprints and are technically irreproducible. These methods require special materials and high production technology, and users need to learn for the identification of anti-counterfeiting patterns.

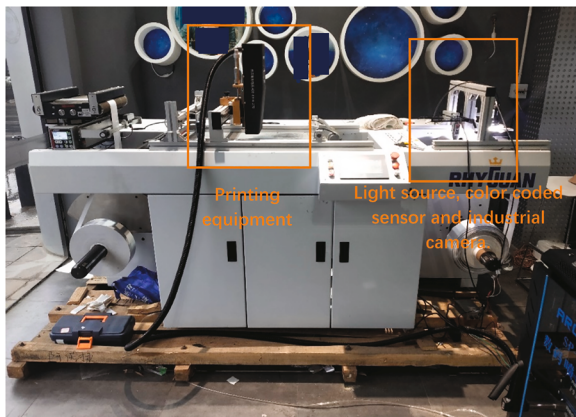


Fig. 3. Ink printing equipment.

Although these anti-counterfeiting technologies have good anti-counterfeiting capabilities, they usually require specific conditions, such as special materials, high-precision scanners, and a large number of sample images. Therefore, anti-counterfeiting strategies that do not require the help of special tools and that are unclonable are the demands of the current problem. For this reason, we have proposed an anti-counterfeiting strategy that mimics fingerprints based on the random diffusion of random inks. The purpose is to overcome the dependence on special materials and a large number of sample images, and it is not technically reproducible.

3. System architecture and workflow

The design of the anti-counterfeiting pattern authenticity identification system takes into account the characteristics of anti-counterfeiting pattern printing, sensor acquisition and deployment, the identification process, and the anti-counterfeiting function requirements and other related factors. It integrates equipment printing, optical lighting, image acquisition, algorithm processing, human-computer interaction and other functions. According to its functions, it can be divided into two main modules: the anti-counterfeiting pattern generation and collection module and the data storage and processing module. Fig. 2 presents the overall framework of the system. The anti-counterfeiting pattern generation and acquisition module is mainly composed of an ink printing system, optical lighting system, camera imaging system and mobile terminal acquisition system. The anti-counterfeiting pattern is generated by a computer that adopts random functions cooperating with the fractal interpolation method to generate a binary anti-counterfeiting pattern with small random textures. The ink printing equipment adopts the Arojet SP-9022 medium-speed variable data inkjet system, as shown in Fig. 3, and the light source is a double-focused LED light source. Additionally, the industrial camera chosen is the Hikvision 5-megapixel industrial array camera with the trigger mode, and a color code sensor is used to collect the images of the anti-counterfeiting pattern samples one by one. For the data storage and processing module, the Alibaba Cloud is adopted as the platform.

4. Proposed method

The main purpose of this paper is to design and develop an effective authenticity identification system for an anti-counterfeiting pattern that can directly extract the most important features of the key regions in the anti-counterfeiting pattern. Because the anti-counterfeiting pattern is composed of randomly generated texture patterns, each anti-counterfeiting pattern is different, and its unique subtle grain and original printing physical features can be very useful against forgeries. Although the forged anti-counterfeiting pattern will have differences in stroke weight, shape and position, the same true anti-counterfeiting

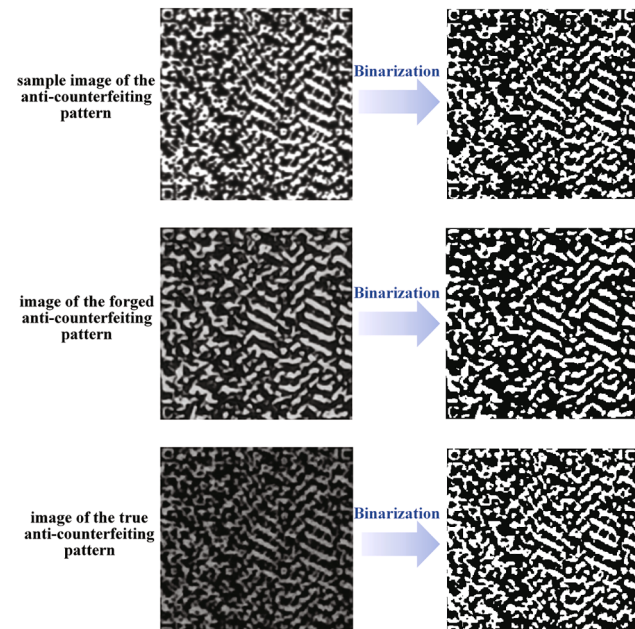


Fig. 4. The binarization effect of the sample images of the anti-counterfeiting pattern and the image of the inspected anti-counterfeiting pattern.

pattern image collected by different devices and environments will also have slight differences, making it difficult to accurately distinguish the true and false images based on the differences directly for the carefully forged anti-counterfeiting pattern. However, the forged anti-counterfeiting pattern inevitably has a forged trace making it different from the true anti-counterfeiting pattern in the subtle region of the anti-counterfeiting pattern, which makes it possible to identify the anti-counterfeiting pattern. Therefore, the focus of this paper is to extract and describe the features of subtle regional differences.

Before identifying the authenticity of anti-counterfeiting patterns, the matching algorithm is used for preprocessing to register and correct the anti-counterfeiting patterns to ensure that the image of the inspected anti-counterfeiting pattern is aligned with the sample images of the anti-counterfeiting pattern (Ma, Zhao, Jiang, Zhou, & Guo, 2019; Zheng et al., 2019).

4.1. Supervised guided segmentation

Image quality is an important factor affecting binary image segmentation. Due to the illumination, posture and shape, the imaging effect of the same anti-counterfeiting pattern varies for different devices, locations and environments. Therefore, the simple binarization algorithm cannot truly restore the details of the anti-counterfeiting pattern, especially the alternating light and dark details of the image. To reduce the distortion of the binary image, guarantee the segmentation accuracy of the anti-counterfeiting pattern, and simultaneously identify the authenticity of the anti-counterfeiting pattern, this paper presents a method that uses the sample binary image of the anti-counterfeiting pattern as the standard supervision model. The binary image of the inspected anti-counterfeiting pattern is generated by guiding threshold correction to improve the quality of the binarization and ensure the accuracy of the segmentation.

4.1.1. Binarization pretreatment

The sample image acquisition environment of the anti-counterfeiting pattern is stable, and the imaging effect is good. Therefore, this article chooses the simple global Otsu threshold segmentation method (Otsu, 1979) to process the sample images of the anti-counterfeiting pattern. For images of the inspected anti-counterfeiting pattern taken in different

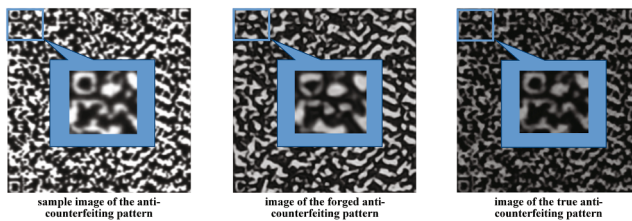


Fig. 5. The difference region of the sample images of the anti-counterfeiting pattern and the image of the inspected anti-counterfeiting pattern.

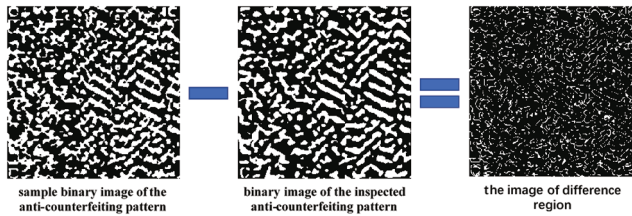


Fig. 6. The extraction effect of different regions.

environments and by different devices, there is a large difference; thus, the low-pass Wiener filter should be used to preprocess the image of the inspected anti-counterfeiting pattern first, and then the Otsu algorithm can be used for binary segmentation. If there are multiple extreme values of interclass variance, the local threshold segmentation method can also be selected for binarization. The binarization effect is shown in Fig. 4.

4.1.2. Difference region extraction

Usually, places that are difficult to counterfeit (namely, regions with good anti-counterfeiting properties) belong to small regions or angular regions. These regions of forged images are prone to rupture or expansion; thus, the true image will also exhibit more or fewer imaging differences under different types of collection equipment or environments, but they will have a certain relevance under a better image quality, as shown in Fig. 5. Therefore, we need to extract the difference region of the inspected image for analysis. To quickly locate the difference region, we directly use the difference between the sample binary image of the anti-counterfeiting pattern and the binary image of the inspected anti-counterfeiting pattern. Part of the difference is caused by the difference in the edge shading transition, and part is caused by the difference in the forged anti-counterfeiting pattern itself. Therefore, we need to extract the difference regions and judge the true attributes of the difference regions.

Due to the accurate registration of the anti-counterfeiting pattern before binarization, it can be considered that the size and position of the sample anti-counterfeiting pattern and the inspected anti-counterfeiting pattern are fully registered. Therefore, we find region D directly by mapping the sample binary image of the anti-counterfeiting pattern to the binary image of the inspected anti-counterfeiting pattern.

$$D(x, y) = \begin{cases} 1 & |SB(x, y) - TB(x, y)| \neq 0 \\ 0 & |SB(x, y) - TB(x, y)| = 0 \end{cases} \quad (1)$$

where $SB(x, y)$ is the sample binary image of the anti-counterfeiting pattern and $TB(x, y)$ is the binary image of the inspected anti-counterfeiting pattern. The different regions are shown in Fig. 6.

4.1.3. Determination of the local threshold based on reference model supervised guidance (Guide-Binary)

For the difference region of the image to be measured, we rejudge the binary condition of this region. Since these difference regions occupy fewer pixels in the whole image, we reuse reference model-based su-

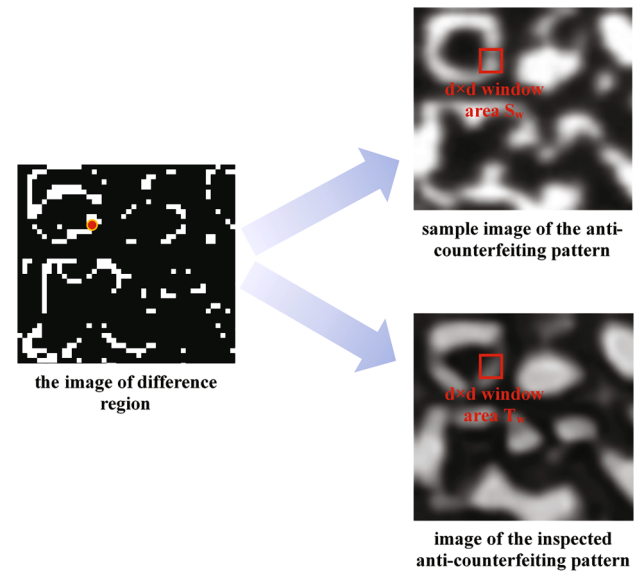


Fig. 7. Window image extraction of the difference regions in the sample image of the anti-counterfeiting pattern and the image of the inspected anti-counterfeiting pattern.

pervision and guidance to obtain the local threshold values for the pixels in the difference regions. We need to regenerate an optimal threshold for each pixel in the difference region. Although it is difficult to accurately binarize the pixels in the difference regions due to illumination, equipment and other reasons, it can still be seen that the difference regions of the two images after the same original image is taken have a certain correlation. To accurately express their correlation, first, each pixel with a value of 1 in the image of the difference region is taken as a window region S_w and T_w with a size of $d \times d$ on the corresponding sample binary image of the anti-counterfeiting pattern and the binary image of the inspected anti-counterfeiting pattern, as shown in Fig. 7. Then, the average gray value and standard deviation of regions S_w and T_w are calculated.

$$\mu_{S_w}(x, y) = \frac{1}{d^2} \sum_{i=x-\frac{d}{2}}^{x+\frac{d}{2}} \sum_{j=y-\frac{d}{2}}^{y+\frac{d}{2}} S(i, j) \quad (2)$$

$$\mu_{T_w}(x, y) = \frac{1}{d^2} \sum_{i=x-\frac{d}{2}}^{x+\frac{d}{2}} \sum_{j=y-\frac{d}{2}}^{y+\frac{d}{2}} T(i, j) \quad (3)$$

$$\sigma_{S_w}(x, y) = \sqrt{\frac{1}{d^2} \sum_{i=x-\frac{d}{2}}^{x+\frac{d}{2}} \sum_{j=y-\frac{d}{2}}^{y+\frac{d}{2}} (S(i, j) - \mu_{S_w}(i, j))^2} \quad (4)$$

$$\sigma_{T_w}(x, y) = \sqrt{\frac{1}{d^2} \sum_{i=x-\frac{d}{2}}^{x+\frac{d}{2}} \sum_{j=y-\frac{d}{2}}^{y+\frac{d}{2}} (T(i, j) - \mu_{T_w}(i, j))^2} \quad (5)$$

where $S(i, j)$ is the sample image of the anti-counterfeiting pattern, $T(i, j)$ is the image of the inspected anti-counterfeiting pattern, and d is the window size.

From the image point of view, there are obvious regional differences between the sample image of the anti-counterfeiting pattern and the image of the inspected anti-counterfeiting pattern, especially in terms of the brightness and contrast difference, but the gray-level distribution has a certain similarity; therefore, we can use the local average deviation (that is, the pixel values used to reduce the average ones) to solve the problem of inconsistent brightness. The contrast difference will affect the volatility of the local average deviation; thus, we consider using the

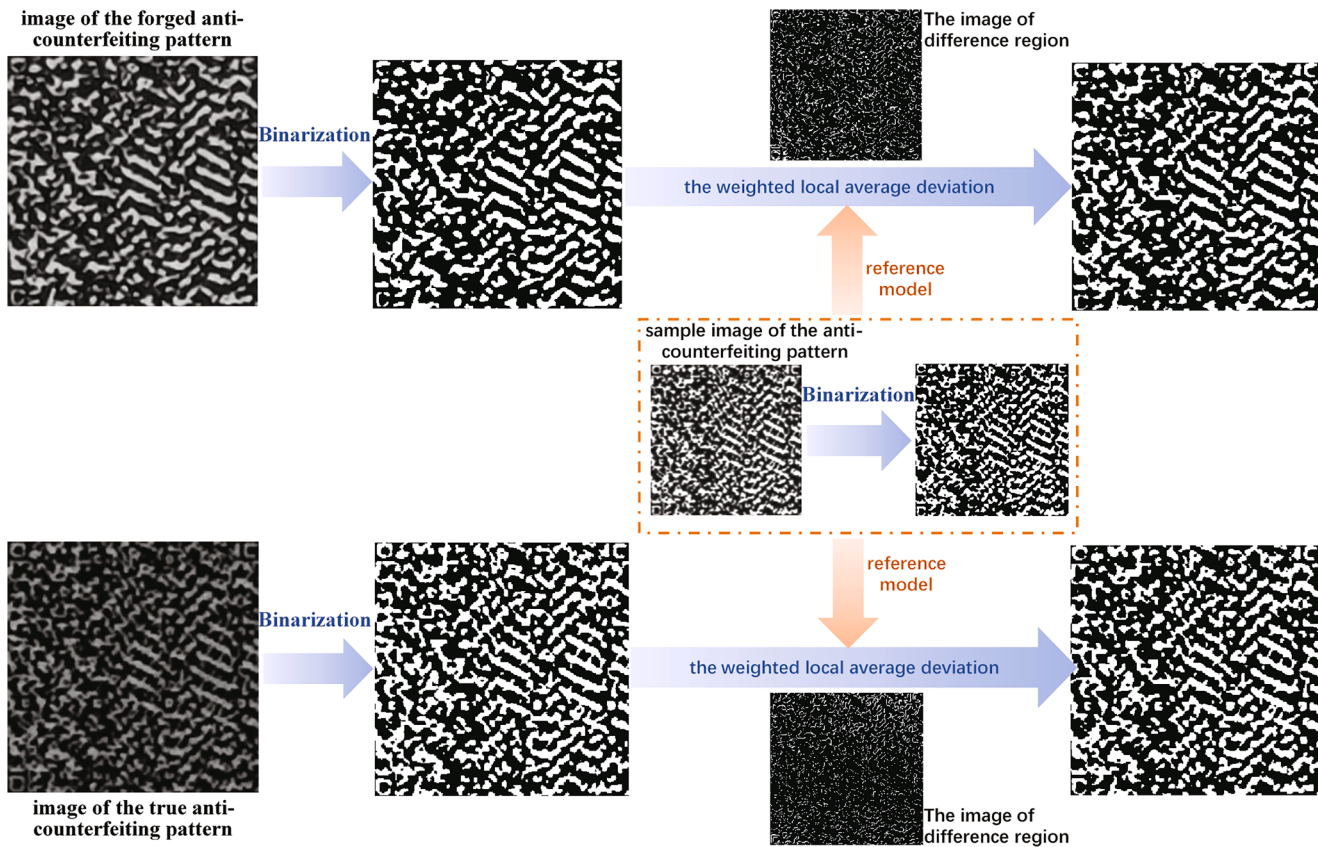


Fig. 8. The binarization effect after supervised boot processing based on the reference model.

weighted local average deviation instead of the local average deviation, according to the local mean and the local standard deviation, to construct the weighted average deviation:

$$U_{S_w}(x, y) = S(x, y) - \mu_{S_w}(x, y) * \left[\frac{\sigma_{S_w}(x, y)}{256} + k \right]^2 \quad (6)$$

$$U_{T_w}(x, y) = T(x, y) - \mu_{T_w}(x, y) * \left[\frac{\sigma_{T_w}(x, y)}{256} + k \right]^2 \quad (7)$$

where k is the correction parameter (usually 1 or 2). We take the weighted local mean deviation $U_{S_w}(x, y)$ of subregion S_w as the reference model. When the weighted local mean deviation $U_{T_w}(x, y)$ of subregion T_w is the same as $U_{S_w}(x, y)$, the distribution of the grayscale is consistent, and the binary effect should be consistent. Otherwise, the binary effect should be reversed. The specific formula is as follows:

$$TB(x, y) = \begin{cases} SB(x, y) & \frac{U_{S_w}(x, y)}{U_{T_w}(x, y)} \geq 0 \\ TB(x, y) & \frac{U_{S_w}(x, y)}{U_{T_w}(x, y)} < 0 \end{cases} \quad (8)$$

After the above operation, the difference region of the image of the inspected anti-counterfeiting pattern is updated to obtain the new image binary map. This method ensures that the image of the inspected anti-counterfeiting pattern is segmented according to the binary effect of the sample image of the anti-counterfeiting pattern as much as possible, and the operation process is shown in Fig. 8.



Fig. 9. The stroke width in the binary image of the anti-counterfeiting pattern.

4.2. Bone Width Transformation(BWT)

Through the observation and analysis of the printing ink, the small background gap between the two inks and the separate subtle ink grains easily caused distortion because of ink adsorption or defects in the printing machinery; therefore, these narrow, long, blank backgrounds or narrow long inks form subtle grains that are difficult to imitate, as shown in Fig. 5. To reduce the influence of the external environment, such as illumination and noise, the subtle region can be extracted directly by using the sample binary image of the anti-counterfeiting pattern. The determination of the subtle regions in the binary images can be represented by the region width. Therefore, this paper proposes BWT to calculate the stroke width of binary images, that is, the distance between the two edges, and analyzes the width and narrowness of the stroke width. The bone width transformation is similar to the stroke width

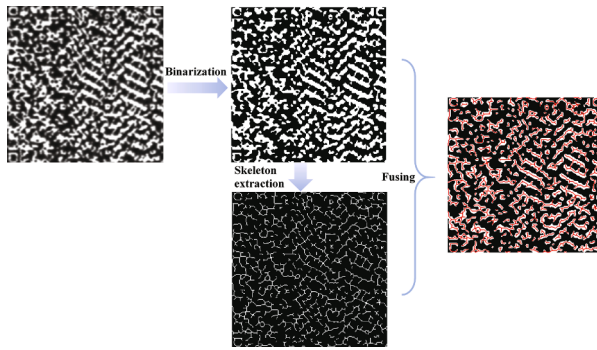


Fig. 10. Skeletal extraction pretreatment of the anti-counterfeiting pattern.

transform (Epshtain, Ofek, & Wexler, 2010) and belongs to the local image operator, which calculates the width of the bone where each pixel is located. As shown in Fig. 9, the white region is the stroke pixels, the black region is the background pixels, and the red line is the stroke width.

First, the skeleton is extracted from the binary image, and then the extracted skeleton image and the binary image are combined to calculate the bone width transformation, as shown in Fig. 10. The skeleton in the white region is extracted and fused into the binary image, and the red line in the fusion image represents the skeleton.

After fusion, the normal direction θ of each point on the skeleton is first obtained, which can be calculated according to the skeleton function $f(x)$. The normal direction of point a on the skeleton can be expressed as:

$$\theta = \begin{cases} \arctan\left(-\frac{1}{f'(a)}\right) & \text{Interior normal direction} \\ \pi - \arctan\left(-\frac{1}{f'(a)}\right) & \text{Exterior normal direction} \end{cases} \quad (9)$$

The skeleton in the image exists in the form of a discrete point set, and its skeleton function requires curve fitting using the point set. Then, the normal direction of each point is calculated. The calculation process is complex and requires a long operation time. Therefore, in this paper, the gradient calculation is carried out on the skeleton to obtain the gradient change value on both sides of the skeleton line, where the gradient calculation can be used in a simple horizontal vertical difference method. The horizontal vertical gradient is used to collect the gradient direction τ . The formula for computation is as follows:

$$\frac{\partial g(i,j)}{\partial x} = g(i,j+1) - g(i,j) \quad (10)$$

$$\frac{\partial g(i,j)}{\partial y} = g(i+1,j) - g(i,j) \quad (11)$$

$$\tau = \arctan\left(\frac{\partial g_y(i,j)}{\partial g_x(i,j)}\right) \quad (12)$$

where $g(i,j)$ is the pixel value of position (i,j) in the skeleton binary image, the gradient direction of the skeleton can be regarded as its normal direction, and the edge point is searched for according to the interior and exterior normal directions. When the background point is searched, the traversal stops, and this point is the required edge point of the skeleton, namely points p and q :

$$\begin{cases} p : B(i - \vec{\tau}, j - \vec{\tau}) = 0 \\ q : B(i + \vec{\tau}, j + \vec{\tau}) = 0 \end{cases} \quad (13)$$

$B(i - \vec{\tau}, j - \vec{\tau})$ and $B(i + \vec{\tau}, j + \vec{\tau})$ are the pixel values after moving along the interior and exterior directions of t in the binary image of the anti-counterfeiting image. The distance between the two edge points p and

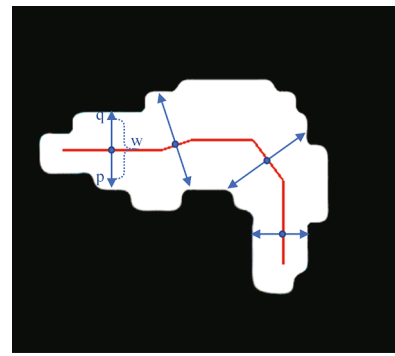


Fig. 11. Processing diagram of BWT in the anti-counterfeiting pattern; the red line is the extracted skeleton, the points p and q are the pixels on the bone boundary, the blue arrow is the normal direction, and w is the bone width.

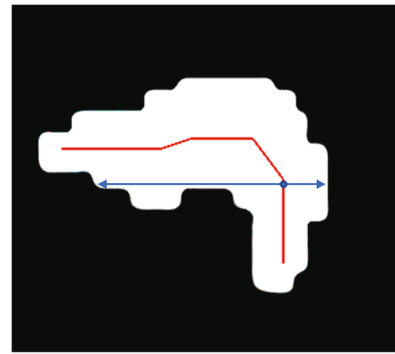


Fig. 12. Abnormal noise points in bone width calculations.



Fig. 13. The distribution of endpoints at the center point of the 3×3 window.

q constitutes the bone width $w = \|q - p\|$, as shown in Fig. 11.

4.3. Feature difference extraction of the key and subtle regions

The bone width transformation provides the width of the pattern texture in the binary image of the anti-counterfeiting image. However, in the process of skeleton extraction, calculation errors will occur at some corners, leading to abnormal calculation of the skeleton width, as shown in Fig. 12. However, the occurrence frequency of these abnormal values is very low, and they can be treated as noise points. In other words, when there is a sharp mutation in the bone width value, the bone width at this point is a noise point, which needs to be denoised.

To extract the subtle region of the anti-counterfeiting pattern, that is, the relatively narrow bone width, the place with a subtle width r could be found based on the bone width values, for example, when the bone width value is less than the width threshold t . This point will serve as a subtle region, which will cause some endpoints to exhibit separate point misjudgment in a small region that takes the width threshold as the only criterion; thus, it is necessary to eliminate these interference points. A single point can be used to make judgments according to the number of connected component points. If only this point is less than the width threshold in the 3×3 window of this point, it is considered to be a separate point for elimination. The endpoint is judged by the

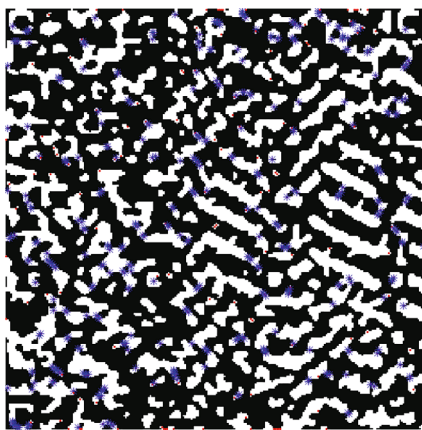


Fig. 14. The key skeleton points of the key and subtle regions of the anti-counterfeiting pattern.

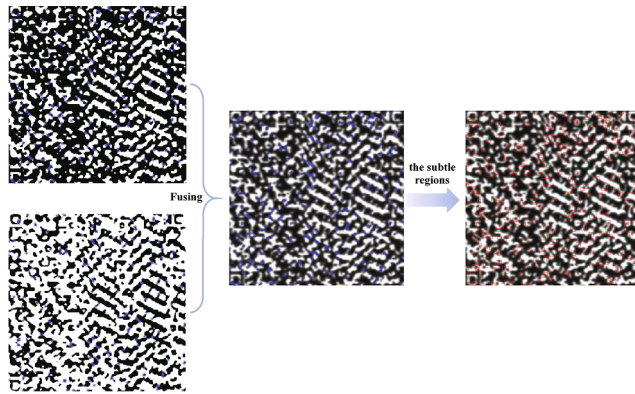


Fig. 15. The subtle regions of the anti-counterfeiting pattern.

distribution rule of the points, that is, there are only three points in the 3×3 window of this point, and the distribution rule of the three points is shown in Fig. 13; then, this point is the endpoint to be eliminated.

Through denoising of the abnormal values and elimination of the endpoints and single points, skeleton points with widths less than the bone width threshold are used as the key points of the subtle region. As shown in Fig. 14, the red points are the removed endpoints and single points, while the blue points are the skeleton key points of the final subtle region. The unit step function $sq(\cdot)$ used to judge the key points of the subtle region is as follows:

$$sq(i,j) = \begin{cases} 1 & d(i,j) \leq t \\ 0 & d(i,j) > t \end{cases} \quad (14)$$

where $d(\cdot)$ is the bone width of the skeleton point, and t is the bone width threshold.

In general, it is easy to break and merge the forged images in the subtle regions; thus, the bone width transformation of the binary image can be used to locate the subtle regions quickly to obtain the differences between the subtle regions. However, bone width transformation can be used to calculate the width only in either the white or black region. To obtain the individual small black ink lines and the small white background gaps, this paper carries out the bone width transformation for both the black region and the white region and then combines the skeleton width values obtained by the two transformations to obtain all the skeleton key points and subtle regions in the whole picture, as shown in Fig. 15.

For the construction of the subtle region, it is not possible to simply construct regions with the skeleton key points, especially the partial narrow and long subtle regions. The skeleton key points whose adjacent

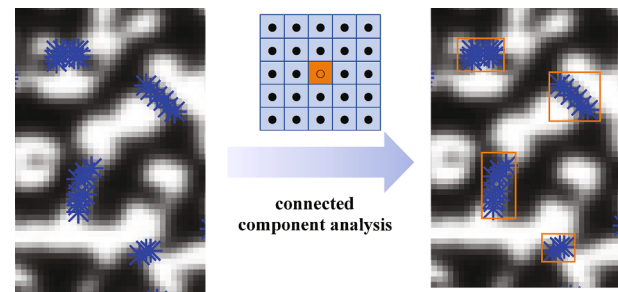


Fig. 16. The subtle region construction process.

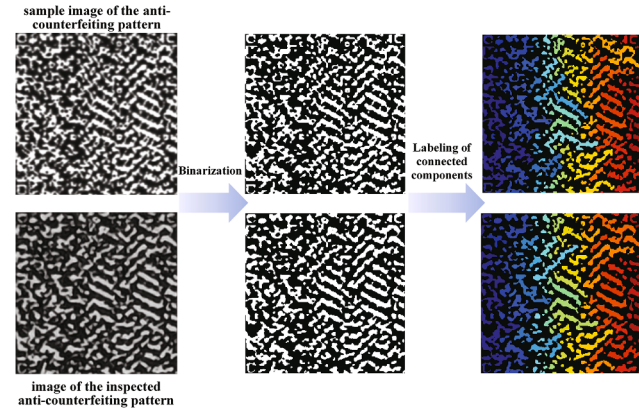


Fig. 17. The labeling of connected components of the binary image of the anti-counterfeiting pattern.

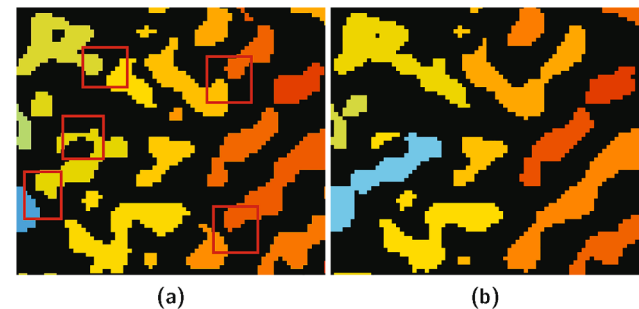


Fig. 18. (a) and (b) are partial images of the sample anti-counterfeiting pattern and the inspected anti-counterfeiting pattern, respectively, with each red box indicating a part of the subtle regions.

points satisfy the conditions can be connected to form a large subtle region, as shown in Fig. 16. Therefore, in this section, a 5×5 template is selected to analyze the connected component, and the skeleton points are connected to determine the size of the connected region. Then, each connected region is structured into a rectangle, and two surrounding pixels are expanded to form the subtle region, which is used for the regional positioning for subsequent identification.

Additionally, to identify the authenticity of the inspected anti-counterfeiting pattern, this section discusses the connectivity component analysis of the 8-neighborhood component for both the sample binary image of the anti-counterfeiting pattern and the binary image of the inspected anti-counterfeiting pattern, as shown in Fig. 17.

Then, connected component analysis and texture difference analysis of the subtle region in the sample image of the anti-counterfeiting pattern and the image of the inspected anti-counterfeiting pattern are carried out to determine the authenticity of the inspected anti-counterfeiting pattern. The connected component analysis counts the

connected labels of each subtle region in the sample binary image of the anti-counterfeiting pattern and the binary image of the inspected anti-counterfeiting pattern and compares them. Usually, narrow subtle strokes in the anti-counterfeiting pattern are disconnected during forgery printing, and two connected components are generally formed. However, the small gap between the strokes is filled during forgery printing, and the two connected components become one connected component. As shown in Fig. 18, it is obvious that the connected regions contained in the red box in figure a and figure b are different.

The difference judgment formula of each subtle region is:

$$CNum(i) = \begin{cases} 1 & NumB_s(i) \neq NumB_d(i) \\ 0 & NumB_s(i) = NumB_d(i) \end{cases} \quad (15)$$

where $NumB_s(i)$ is the number of connected labels of the sample binary image of the anti-counterfeiting pattern and $NumB_d(i)$ is the number of connected labels of the binary image of the inspected anti-counterfeiting pattern in the i^{th} subtle region.

When the number of differences in the subtle regions of the inspected anti-counterfeiting pattern exceeds a certain threshold, it can be considered a forged anti-counterfeiting pattern.

$$CS = \begin{cases} \text{true} & \sum CNum(i) \leq \rho \\ \text{false} & \sum CNum(i) > \rho \end{cases} \quad (16)$$

The difference quantity sum is expressed by $\sum CNum(i)$, and ρ is the judgment threshold value.

The texture difference analysis extracts the LBP mode texture features of all the subtle regions in the sample grayscale image of the anti-counterfeiting pattern and the grayscale image of the inspected anti-counterfeiting pattern, counts the feature histograms of each subtle region, and calculates the similarity distance. The distance formula is as follows:

$$d(j) = \sqrt{\sum_{i=0}^{N_{\text{bin}}-1} (hist_s^j(i) - hist_d^j(i))^2} \quad (17)$$

where $hist_s^j(i)$ and $hist_d^j(i)$ are the texture feature histograms of the j^{th} subtle region in the sample grayscale image of the anti-counterfeiting pattern and the grayscale image of the inspected anti-counterfeiting pattern, respectively. Then, we judge whether there is an obvious difference:

$$LNum(j) = \begin{cases} 1 & d(i) > \kappa \\ 0 & d(i) \leq \kappa \end{cases} \quad (18)$$

where κ is the judgment threshold; the authenticity judgment based on the texture difference is as follows:

$$LS = \begin{cases} \text{true} & \sum LNum(i) \leq \omega \\ \text{false} & \sum LNum(i) > \omega \end{cases} \quad (19)$$

where ω is the judgment threshold. When one of the connected component analyses and texture difference analyses detects a forgery, the pattern is finally considered a forged anti-counterfeiting pattern:

$$SS = \begin{cases} \text{true} & CS = \text{true} \cap LS = \text{true} \\ \text{false} & CS = \text{false} \cup LS = \text{false} \end{cases} \quad (20)$$

5. Experimental results and analysis

In this section, we present experiments to verify the proposed method. The experiments are performed on newly created data sets, on which all the rendering methods are tested and evaluated.

Table 1

The printers used in the experiment.

Printer brand	Printer model	Dots Per Inch(dpi)	Printing type
HP	M281fdw	600 * 600	LaserJet
HP	M436n	600 * 600	LaserJet
HP	M1136	600 * 600	LaserJet
HP	P1106	600 * 600	LaserJet
HP	DJ5078	1200 * 1200	Inkjet
Canon	MF525dw	600 * 600	LaserJet
Canon	E568	4800 * 1200	Inkjet
EPSON	L3118	5760 * 1440	Inkjet
SAMSUNG	C480W	600 * 600	LaserJet
Lenovo	M7268W	600 * 600	LaserJet

Table 2

The mobile phones used in the experiment.

Mobile phone brand	Mobile phone model	Physical pixel
APPLE	6s	12 million
APPLE	6s Plus	12 million
APPLE	7	12 million
APPLE	8 Plus	12 million
HUAWEI	Mate 20 Pro	40 million
HUAWEI	Honor20	48 million
OPPO	K1	16 million
VIVO	IQOO	12 million
MI	Redmi Note 7	48 million
MEIZU	16	20 million

5.1. Data sets and experimental settings

To verify the performance of the algorithm designed in this paper, the parameters of the algorithm are kept consistent throughout the experiment. The experiments were carried out on a laptop with a 2.4-GHz i7 Intel core CPU, 8 GB of memory and the Windows 10 operating system, and the algorithms were implemented using MATLAB @r2016a.

At present, there is little research literature on one-to-one anti-counterfeiting and no related public data sets, thus, we built our own anti-counterfeiting pattern data set. First, the ink printing equipment of the system is used to print 20 different samples of anti-counterfeiting patterns, and the sample digital images are collected by the system camera. Then, 10 laser and ink jet copy printers of different brands (Table 1) are used to print or copy these 20 different anti-counterfeiting patterns for forgery sampling. Each printer copies or prints one copy of each sample anti-counterfeiting pattern, with a total of 20 groups. Each group contains 10 forged anti-counterfeiting patterns, and the total number of counterfeit patterns is 200. Finally, 10 mobile phones of different brands (Table 2) are used to take photos of the 20 sample anti-counterfeiting patterns and the 200 forged anti-counterfeiting patterns. Therefore, this data set is composed of 20 sets of data; each set of data includes 1 sample image, 10 true inspected images and 100 forged inspected images. Among them, the backgrounds of the inspected images are different categories of cigarettes, drugs and alcohol.

Although the anti-counterfeiting pattern is randomly generated by the computer, it needs to contain 300–400 subtle areas. Additionally, the anti-counterfeiting pattern after registration will be normalized to a fixed size. Therefore, through the analysis of the printer's printing accuracy and image acquisition, the bone width threshold is determined to be the printing width of ten ink dots divided by the actual size of the printing, and then multiplied by the size of the anti-counterfeit pattern image. In this paper, the bone width threshold t is set to 3. The threshold ρ of the number of subtle areas with differences is determined by 10% of the total subtle areas.

Table 3
Segmentation effects of different binarization algorithms

	Original image	Otsu	Gatos	Genetic-Otsu	Gravitation Search	Proposed
Sample						
Iphone6s true						
Huawei-Mate20P true						
Iphone6s forge						
Huawei-Mate20P forge						

5.2. Experimental results

5.2.1. Comparison with binary algorithms

This paper compares the Otsu algorithm, Gatos algorithm (Gatos, Pietikainen, & Perantonis, 2006), genetic-Otsu algorithm (Pruthi & Gupta, 2016) and gravitation search algorithm (Qi & Ma, 2017) with our guide-binary algorithm. Before the binarization of the image of the inspected anti-counterfeiting pattern, the corrected anti-counterfeiting pattern image is first obtained by registration, and the size is normalized to 256×256 . In this paper, the anti-counterfeiting pattern forged by the Canon E568 printer is selected as an example to show the segmentation effect of each binarization algorithm (Table 3). The second row in the table presents the binarization effect of the sample image, the third row to the fourth row present the true inspected images, and the fifth row to the sixth row present the forgery inspected images, which are collected by 2 different mobile phones.

From the experimental results in this table, because of the different acquisition environments and different collection effects on different cell phones, the image quality is uneven, leading to the segmentation results of the forged images and the true anti-counterfeiting pattern image not being satisfactory, as obtained by the Otsu algorithm, Gatos algorithm, genetic-Otsu algorithm and gravitation search algorithm. There are large differences compared with the sample binary image. For example, the small regions of the black strokes in the upper left corner are broken, and the dense regions in the middle are bonded. The difference between the true and forged anti-counterfeiting patterns cannot be distinguished in this region, which will seriously affect the

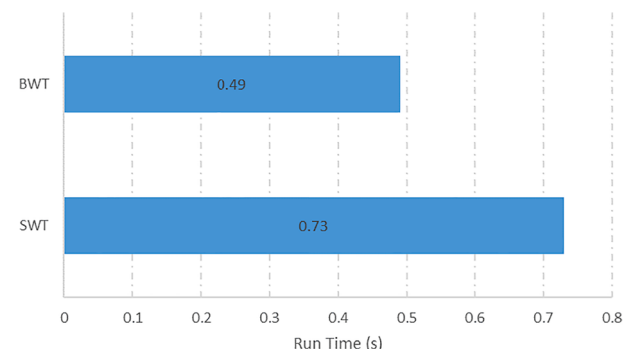


Fig. 19. Time-consuming comparison between the Bone Width Transformation (BWT) algorithm and the Stroke Width Transformation (SWT) algorithm.

subsequent identification of authenticity. However, the segmentation results of the guide-binary algorithm can accurately restore the true anti-counterfeiting pattern image, and all the images in the experiment have no obvious distortion, clearly reflecting the difference between the image of the forged anti-counterfeiting pattern and that of the sample anti-counterfeiting pattern as well as the consistency between the true and sample anti-counterfeiting pattern images.

5.2.2. Comparison with width extraction algorithms

To verify the effectiveness of the BWT algorithm, it will be compared

Table 4

Performance comparison.

Anti-counterfeiting algorithm	Precision	Recall	F1-measure
GLCM	76%	68%	66%
LBP	71%	70%	65%
MRELBP	79%	80%	80%
RALBGC	85%	83%	84%
Proposed	97%	91%	94%

with the stroke width transformation (SWT) algorithm. Since the application scenarios are different, the algorithm time is taken as the main comparison. Since binarization preprocessing is required in the early stage, we uniformly adopt the guide-binary algorithm and the above data set for preprocessing, as shown in Fig. 19. The SWT needs to calculate the gradient direction of the corresponding edge, that is, the gradient direction needs to be calculated twice. However, BWT only needs to calculate the skeleton gradient direction once, which has obvious advantages in time consumption.

5.2.3. Comparison with anti-counterfeiting algorithms

Precision rate and recall rate:

Precision and recall are usually used to evaluate the performance of an algorithm.

$$\text{Precision} = \frac{tp}{tp + fp} \quad (21)$$

$$\text{Recall} = \frac{tp}{tp + fn} \quad (22)$$

where tp is the number of true anti-counterfeiting patterns correctly recognized, fp is the number of forged anti-counterfeiting patterns incorrectly recognized, and fn is the number of true anti-counterfeiting patterns incorrectly recognized.

In the process of authenticity identification, there are few studies on one-to-one identification methods. To show the effectiveness of the proposed algorithm in this paper, we compare it with relevant texture feature identification algorithms such as the LBP, GLCM, MRELBP (Liu

et al., 2016) and RALBGC (El Khadiri, Kas, El Merabet, Ruichek, & Touahni, 2018), where these four texture features are calculated using the full image. Table 4 summarizes the experimental results of the precision rates and recall rates of each anti-counterfeiting algorithm for the 20 data sets. It can be seen from the table that the average precision rate of this algorithm is over 97%, which can better tolerate the differences between the images of the true anti-counterfeiting patterns caused by the different collection devices. Compared with the four texture features, the main advantage of this algorithm is that it can quickly locate the difference regions while eliminating some interference from external factors. Although the difference between the forged anti-counterfeiting pattern and the sample anti-counterfeiting pattern is not obvious, this algorithm is different from the block statistical method of texture features, which can accurately identify subtle differences in specific locations, and the average recall rate is over 90%.

Stability: In the process of authenticity identification of the anti-counterfeiting patterns, it is usually expected that the more similar the image of the true anti-counterfeiting pattern is to the image of the sample anti-counterfeiting pattern, the better, while the more different the forged anti-counterfeiting pattern is to the image of the sample anti-counterfeiting pattern, the better. Therefore, to better show the discernibility of the algorithms, the difference values of the inspected anti-counterfeiting patterns are displayed as scatter plots, as shown in Fig. 20. We list the test results of ten data sets for a sorting display. The solid line in the figure is the image of the forged anti-counterfeiting pattern, the dotted line is the image of the true anti-counterfeiting pattern, the x coordinate is the serial number of the anti-counterfeiting pattern, and the y coordinate is the calculated difference value. The smaller the difference value is, the more similar the region is. Our algorithm can ensure that there is an obvious distance between the difference values of the true anti-counterfeiting pattern and the forged anti-counterfeiting pattern. In reality, it is usually not allowed to misjudge forged products as genuine; thus, the judgment conditions can be set more strictly.

To express the separability more intuitively from the data, the measurable Mann–Whitney U test method can be used to judge whether there is a significant difference between the two types of data. The

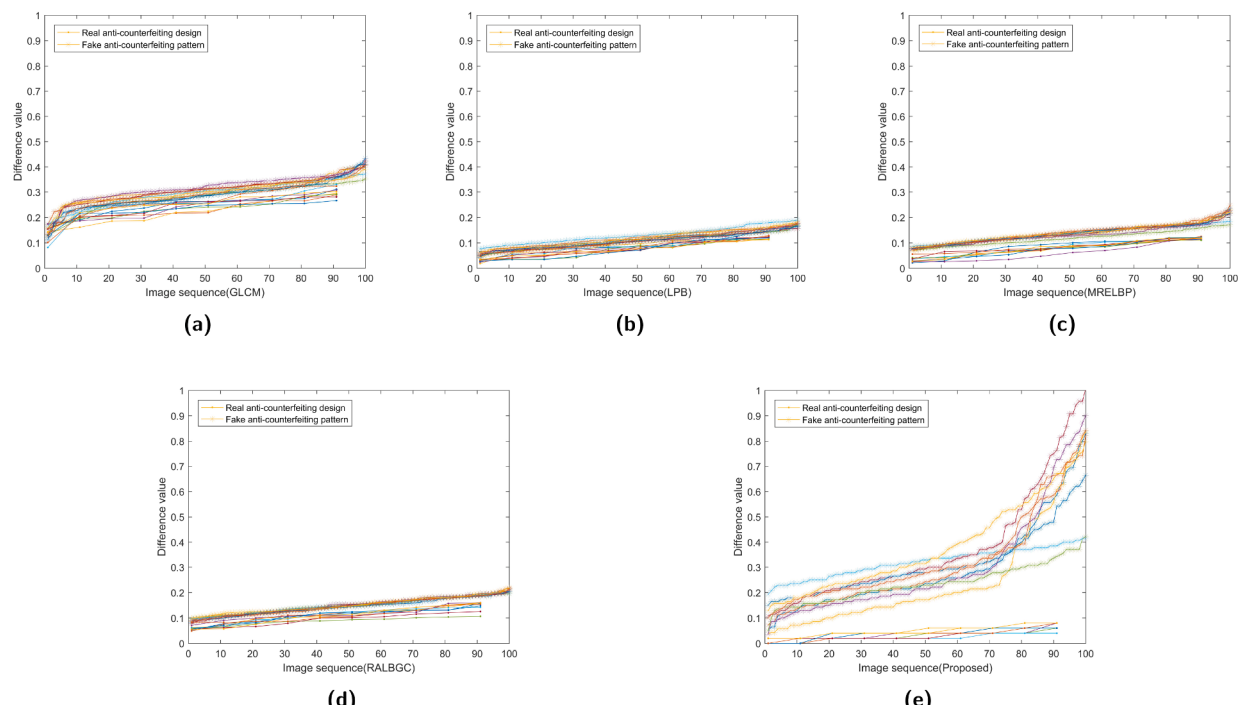


Fig. 20. Scatter diagram of the difference values.

Table 5
U-value comparison.

Anti-counterfeiting algorithm	U-Value
GLCM	11.6
LBP	10.7
MRELBP	18.1
RALBGC	13.4
Proposed	46.1

calculation formula of the U value is as follows:

$$U = \frac{|u_1 - u_2|}{\sqrt{\frac{\sigma_1^2}{n} + \frac{\sigma_2^2}{n}}} \quad (23)$$

where u_1 and u_2 are the mean values of the true and forged anti-counterfeiting patterns and σ_1 and σ_2 are the standard deviations of the true and forged anti-counterfeiting patterns, respectively.

Generally, the larger the mean difference between the two types of data is, the easier it is to distinguish them, and the smaller the data variance is, the lower the volatility is and the less prone it is to misjudgment. However, the larger the U value of the Mann–Whitney U test is, the larger the mean difference is and the smaller the variance is. According to the experimental data, Table 5 shows that our algorithm has good separability and performance stability.

6. Conclusion

The usual anti-counterfeiting technology is to add special materials or professional detection equipment. Due to the high cost or complicated user identification steps, the effect is greatly discounted in practical applications. This paper proposes an automatic identification method for the authenticity of anti-counterfeit patterns based on the random diffusibility of ink to solve the dependence on anti-counterfeit materials. Compared with the previous anti-counterfeiting identification methods, our method has two advantages. (1) A random fingerprint-like pattern image as an anti-counterfeiting pattern is developed and combined with the randomness of ink diffusion to ensure that it is technically non-reproducible. (2) The supervised guided segmentation algorithm and the bone width transformation algorithm can quickly locate the key areas of anti-counterfeiting, thereby replacing large samples of images for training or manual observation. This method has high credibility and discriminability in the identification of anti-counterfeiting patterns. However, this method requires anti-counterfeiting patterns with specific random textures, which has limitations in application. The next step will focus on the research of arbitrary patterns. Additionally, the robustness of the image quality will be improved so that this method can achieve a better effect on special poor environments.

CRediT authorship contribution statement

Zhaohui Zheng: Conceptualization, Methodology, Software, Writing - original draft, Formal analysis. **Hong Zheng:** Project administration, Conceptualization. **Jianping Ju:** Visualization. **Deng Chen:** Data curation. **Xi Li:** Resources. **Zhongyuan Guo:** Software. **Changhui You:** Writing - review & editing. **Mingyu Lin:** Writing - review & editing.

Declaration of competing interest

The authors declare that they have no known competing financial interests or personal relationships that could have appeared to influence the work reported in this paper.

Acknowledgments

This work was supported in part by the Science and Technology Research Project of Hubei (China) Education Department (No. B2019409), the Wuhan Railway Vocational College Bidding Foundation of China (No. QZB2020001) and the Program for Innovative Research Team in Wuhan Railway Vocational College of Technology.

References

- Alizadeh, R., Allen, J. K., & Mistree, F. (2020). Managing computational complexity using surrogate models: a critical review. *Research in Engineering Design*, 31, 275–298.
- Bae, H., Bae, S., Park, C., et al. (2015). Biomimetic micro fingerprints for anti-counterfeiting strategies. *Advanced Materials*, 27, 2083–2089.
- Cheng, L. Y. (2015). *Automatic identification algorithm of texture anti-counterfeiting tag base on transform domain*. Hainan University.
- El Khadiri, I., Kas, M., El Merabet, Y., Ruichek, Y., & Touahni, R. (2018). Repulsive-and-attractive local binary gradient contours: new and efficient feature descriptors for texture classification. *Information Sciences*, 467, 634–653.
- Elkasrawi, S., & Shafait, F. (2014). Printer identification using supervised learning for document forgery detection. The 11th IAPR International Workshop on Document Analysis Systems (pp. 146–150).
- Epshtain, B., Ofek, E., & Wexler, Y. (2010). Detecting text in natural scenes with stroke width transform. In *2010 IEEE Conference on Computer Vision and Pattern Recognition* (pp. 2963–2970). <https://doi.org/10.1109/CVPR.2010.5540041>
- Ferreira, A., Navarro, L. C., Pinheiro, G. R., dos Santos, J. A., & Rocha, A. (2015). Laser printer attribution: Exploring new features and beyond. *Forensic Science International*, 247, 105–125.
- Gatos, B., Pietikäinen, I., & Perantonis, S. J. (2006). Adaptive degraded document image binarizations. *Pattern Recognition*, 39, 317–327.
- Gebhardt, J., Goldstein, M., Shafait, F., et al. (2013). Document authentication using printing technique features and unsupervised anomaly detection. In *2013 12th International Conference on Document Analysis and Recognition* (pp. 479–483).
- He, J. (2010). *Research on new method for seal imprint verification*. Tianjin University.
- Hou, J., Zhang, H., Su, B., et al. (2016). Four-dimensional screening anti-counterfeiting pattern by inkjet printed photonic crystals. *Chemistry - An Asian Journal*, 11, 2680–2685.
- Lampert, C. H., Mei, L., & Breuel, T. M. (2006). Printing technique classification for document counterfeit detection. In *2006 International Conference on Computational Intelligence and Security* (pp. 639–644).
- Liu, L., Lao, S. Y., Fieguth, P. W., Guo, Y., Wang, X. G., & Pietikäinen, M. (2016). Median robust extended local binary pattern for texture classification. *IEEE Transactions on Image Processing A Publication of the IEEE Signal Processing Society*, 25, 1368–1381.
- Liu, M., & Xu, L. P. (2013). Application on packaging anti-counterfeiting technology of cosmetics. *Applied Mechanics and Materials*, 469, 383–386.
- Ma, J. Y., Zhao, J., Jiang, J. J., Zhou, H. B., & Guo, X. J. (2019). Locality preserving matching. *International Journal of Computer Vision*, 127, 512–531.
- Mikkilineni, A., Chiang, P. J., et al. (2005). Printer identification based on graylevel co-occurrence features for security and forensic applications. *Proceedings of SPIE - The International Society for Optical Engineering*, 568, 430–440.
- Navarro, L. C., Navarro, A. K., et al. (2018). Connecting the dots: Toward accountable machine-learning printer attribution methods. *Journal of Visual Communication and Image Representation*, 53, 257–272.
- Otsu. (1979). A threshold selection method from gray-level histograms. *IEEE Transactions on Systems, Man and Cybernetics*, 9, 62–66.
- Pruthi, J., & Gupta, G. (2016). Image segmentation using genetic algorithm and otsu. In *Fifth International Conference on Soft Computing for Problem Solving* (pp. 473–480).
- Qi, N., & Ma, Z. W. (2017). Image segmentation based on the universal gravitation search algorithm. *Journal of Terahertz Science and Electronic Information Technology*, 15, 475–479.
- Schreyer, M., Schulze, C., Stahl, A., & Effelsberg, W. (2009). Intelligent printing technique recognition and photocopy detection using digital analysis for forensic document examination. *Proc. Informatiktag: Fachwissenschaftlicher Informatik-Kongress*, 8, 39–42.
- Sharad, J., & Khanna, N. (2018). Single classifier-based passive system for source printer classification using local texture features. *IEEE Transactions on Information Forensics and Security*, 13, 1603–1614.
- Sharad, J., & Khanna, N. (2019). Source printer classification using printer specific local texture descriptor. *IEEE Transactions on Information Forensics and Security*, 15, 160–171.
- Soltanisehat, L., Alizadeh, R., Hao, H., et al. (2020). Technical, temporal, and spatial research challenges and opportunities in blockchain-based healthcare: A systematic literature review. *IEEE Transactions on Engineering Management*, 99, 1–16.
- Tsai, M. J., Hsu, C. L., Yin, J. S., & Yuadi, I. (2015). Japanese character based printed source identification. In *2015 IEEE International Symposium on Circuits and Systems (ISCAS)* (pp. 2800–2803).
- Tsai, M. J., Yin, J. S., Yuadi, I., & Liu, J. (2014). Digital forensics of printed source identification for chinese characters. *Multimedia Tools and Applications*, 73, 2129–2155.
- Umadevi, M., Agarwal, A., & Rao, R. (2011). Printed text characterization for identifying print technology using expectation maximization algorithm. In *The 5th international conference on Multi-Disciplinary Trends in Artificial Intelligence* (pp. 201–212).

- Wu, H., Kong, X., & Shang, S. (2015). A printer forensics method using halftone dot arrangement model. In *IEEE China Summit & International Conference on Signal and Information Processing 1* (pp. 861–865).
- Wu, S., Liu, B., Su, X., et al. (2017). Structural color patterns on paper fabricated by inkjet printer and their application in anticounterfeiting. *Journal of Physical Chemistry Letters*, 8, 2835–2841.
- Zhang, Y. (2017). *A research of automatic identification algorithm of authentic work anti-counterfeiting label*. Hainan University.
- Zheng, Z. H., Zheng, H., et al. (2019). Feedback unilateral grid based clustering feature matching for remote sensing image registration. *Remote Sensing*, 11, 1418–1429.
- Zhong, K., Li, J., Liu, L., et al. (2018). Instantaneous, simple, and reversible revealing of invisible patterns encrypted in robust hollow sphere colloidal photonic crystals. *Advanced Materials*, 30, 1707246.